Structures and Phase Transformations of Asymmetric Bent Main-Chain Liquid Crystalline Polyesters

Kwang-Un Jeong,[†] Brian S. Knapp,[†] Jason J. Ge,[†] Shi Jin,[‡] Matthew J. Graham,[†] Huiming Xiong,[†] Frank W. Harris,[†] and Stephen Z. D. Cheng*,[†]

Maurice Morton Institute and Department of Polymer Science, The University of Akron, Akron, Ohio 44325-3909, and Department of Chemistry, College of Staten Island, The City University of New York, Staten Island, New York 10314

Received June 28, 2005; Revised Manuscript Received July 29, 2005

ABSTRACT: A series of new asymmetric bent main-chain liquid crystalline (LC) polyesters (BPE-C*n*) were synthesized through the condensation polymerization of A−B type asymmetric α,ω-carboxylic acid−hydroxyl-terminated monomers containing different even numbers of methylene spacers (BPCA-C*n*-P*m*OH, where $n = 6$, 8, and 10). Differential scanning calorimetry results showed three phase transition processes in this series of BPE-C*n* samples. The phase change with the lowest transition temperature is cooling rate dependent, while the two higher temperature transitions are cooling rate independent. One-dimensional (1D) powder wide-angle X-ray diffraction (WAXD) results at different temperatures revealed that during cooling this series of polymers exhibits a low-ordered LC phase and a highly ordered smectic crystal phase before developing a crystalline phase at lower temperatures. The phase structures and symmetry were identified by 2D WAXD and selected area electron diffraction (SAED). On the basis of 2D fiber WAXD patterns, the low ordered LC phase was identified to be an anticlinically tilted SmC (SmC_A) phase, which was constructed by an alternating synclinic SmC phase in each chemical repeating unit layer along the fiber drawn direction. The highly ordered smectic phase was an anticlinically tilted SmH (SmH_A) phase, which was again constructed by an alternating synclinic SmH phase in neighboring layers. On the basis of the crystallographic point of view, this smectic crystal phase had an orthorhombic unit cell. The crystalline structure was determined to be an orthorhombic unit cell (K_O) with $Pna2_1$ symmetry in these three polyesters. The crystalline structures and symmetry were also confirmed by SAED experiments. As the number of methylene units increased, the dimensions of the crystal structures also increased, yet they retained a zigzag conformation. A two-chain packing model of the K_O phase with four chemical repeating units was proposed on the basis of the experimental diffraction patterns and qualitatively supported by simulated structural diffractions. Additionally, the phase identifications were also supported by the observation of texture changes in polarized light microscopy. Even though the zigzag molecular arrangement remains in the low ordered SmC_A and the highly ordered SmH_A phases which mimics the bent-core small molecules, chiral characteristics such as helical supramolecular structures are not observed due to the covalent bonding connections in this series of BPE-C*n* polymers.

Introduction

Thermotropic liquid crystalline (LC) polymers have been interesting subjects for both academic and industrial research because of their anisotropic structures and properties. To achieve the desired physical properties, LC polymers with various chemical structures and molecular architecture including both the mesogenic groups and flexible spacers have been designed.[1−12] Commonly observed modifications include tailoring LC stabilities by selecting different mesogenic groups, different lengths of flexible spacers, and different locations of the mesogens in the LC polymers.

The well-known odd−even effect of the methylene units in LC polymers is originally described as affecting their thermodynamic properties such as the transition temperatures. However, it has also been found that in some main-chain LC polymers the odd−even effect of the flexible methylene units can be observed in their structures and physical properties. For example, the even-numbered main-chain polyesters (BB-*n*, *n* = the number of methylene units) polymerized via the melt condensation of A−A and B−B type monomers, *p*,*p*-bibenzoic acid, and alkylene glycols exhibited a low ordered smectic A (SmA) phase, but the mesophase of the odd-numbered ones was identified to be an anticlinically tilted smectic C (SmC_A) phase.[13−20]

A few years ago, a series of chiral polyesters were designed and synthesized via the solution condensation polymerization of nonracemic chiral A−B type monomers, (*R*)-(−)-4′-{ω-[2-(*p*-hydroxy-*o*-nitrophenyloxy)-1-propyloxy]-1-nonyloxy}-4-biphenylcarboxylic acid [PET-(R*)-*n*, *n* = the number of methylene units]. This series of polymers exhibited an important chiral characteristic, a double-twisted helical single crystal. It is surprising that the handedness of the helical sense in this series of polymers is determined not only by the configurational chirality but also by the number of methylene units.[21−29] For example, having the identical R* chiral center, the even- or odd-numbered methylene units in PET(R*)-*n* switched the helical single crystals from right-handed for *n* = odd to left-handed for *n* = even. This demonstrated a morphological odd−even effect. The chirality transfer between different length scales has been determined to be dependent upon the packing scheme within each of the length scales.[26,28]

To achieve chiral characteristics from achiral molecules, low molecular weight bent-core (banana-shaped) LC molecules with a *meta*-substituted unit at the center of the mesogen have been synthesized. Some of the most

[†] The University of Akron.
[‡] The City University of New York.
* To whom correspondence should be addressed. E-mail: scheng@uakron.edu.

10.1021/ma051389j CCC: $30.25
Published on Web 08/30/2005

fascinating results from these achiral banana-shaped molecules is the formation of helical supramolecular structures in the B7 phase and the spontaneous macroscopic electric polarization in the B2 phase.[30−34] These chiral characteristics were previously thought to only originate from chiral molecules in the SmC* phase. Polymers and the subsequent networks incorporating bent-core mesogenic units have recently been made.[35−40] When the bent-core mesogenic units are attached to the side or end of the fairly flexible backbone systems such as a carbosilane dendrimer[35] or poly(siloxane),[36] ferroelectric polarization was observed in the B2 phase.

We recently reported that a three-dimensional (3D) helical supramolecular structure formed in a smectic C (SmC) phase of a series of 4′-[6-(3′-hydroxylphenoxy)-hexyloxy]-4-biphenylcarboxylic acid compounds with different methylene spacer units (BPCA-C*n*-P*m*OH, $n = 6-10$). This series of compounds was synthesized via four-step substitution reactions. They have neither molecular chirality nor a significant bend like the banana-shaped molecules. On the basis of our experimental observations and computer calculations, we concluded that the helical supramolecular structures in these achiral 4-biphenylcarboxylic acid compounds result from chiral axial conformers of individual head-to-head dimers with a phenyl group at both ends during the transition from the SmA → SmC phases.[41]

The question is: can we design and synthesize a series of asymmetric bent main-chain LC polymers to study their chiral characteristics? Several reports have appeared where the mesogens have symmetric bent-cores.[37−40] The approach we have taken is to use the condensation polymerization of A−B type asymmetric BPCA-C*n*-P*m*OH monomers with different methylene units (*n*). The corresponding polyesters are abbreviated BPE-C*n*. The bend introduced in BPE-C*n* is located at the end of the mesogen by the *meta*-linkage. In this report, the phase structures of this series of BPE-C*n* are identified by wide-angle X-ray diffraction (WAXD) and selected area electron diffraction (SAED). Their molecular conformations and packing schemes were deduced from structural characterization and supported by computer simulations. The phase morphologies in the LC and crystalline phases were investigated via polarized light microscopy (PLM). Differential scanning calorimetry (DSC) experiments were utilized to detect the thermal transitions in this series of BPE-C*n* samples. From these, we achieved an understanding of the mechanisms involved in these structural and morphological formations and their effects on determining chiral characteristics.

Experimental Section

Materials and Sample Preparations. A series of asymmetric bent main-chain LC polyesters (BPE-C*n*) with an even number of methylene units ($n = 6$, 8, and 10) were synthesized via the condensation polymerization of the A−B type asymmetric BPCA-C*n*-P*m*OH (where $n = 6$, 8, and 10), which were prepared via four-step substitution reactions as shown in Scheme 1. Chemical structures of the BPCA-C*n*-P*m*OHs and their corresponding polyesters (BPE-C*n*) were confirmed by Fourier transform infrared spectroscopy (FT-IR) and solution proton (^{1}H) and carbon-13 (^{13}C) nuclear magnetic resonance (NMR). The number-average molecular weights of BPE-C*n* (*n* = even numbers) were determined by gel permeation chromatography (GPC) based on polystyrene standards, and they ranged between 20 000 and 30 000 g/mol with polydispersities between 1.8 and 2.4. The thermal gravimetric analysis (TGA) showed that the BPE-C*n* polyesters were thermally stable. The

Scheme 1

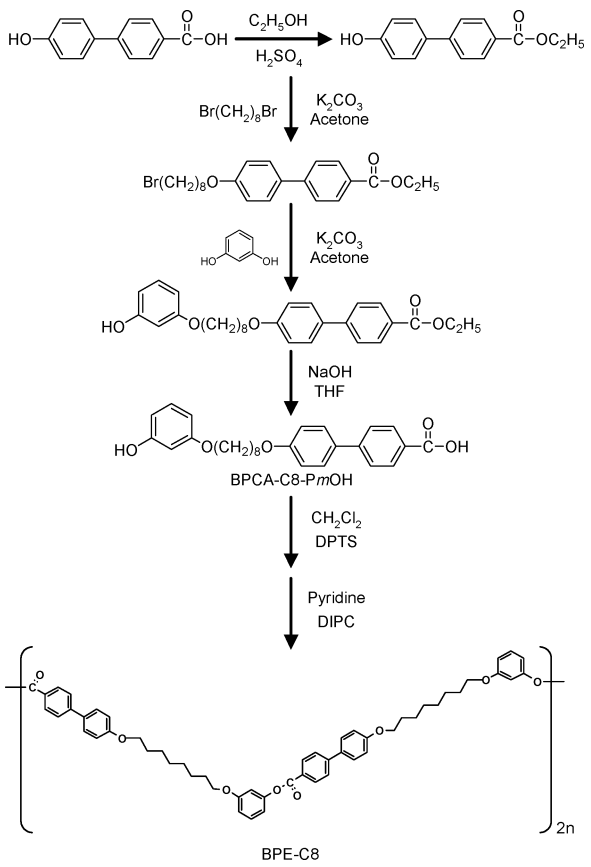

polymer underwent 2% and 5% weight loss at 362 and 392 °C, respectively, at a heating rate of 10 °C/min under a dry nitrogen atmosphere. A more detailed description of the synthetic and purification processes for the monomers and their corresponding polyesters can be found in ref 42.

The samples were kept in a vacuum before carrying out characterization and analysis. For differential scanning calorimetry (DSC) experiments, the sample weight was about 2.0 mg, and the pan weights were kept constant at a precision of ±0.001 mg. To observe the evolution of different phase structures, film samples with a thickness of 1 mm were prepared by melting the polymer powders for one-dimensional (1D) WAXD powder experiments. To prepare oriented fibers for 2D WAXD experiments, samples were first heated to the low ordered LC phase. They were uniaxially drawn from the LC phase to form oriented fibers. The fibers were then annealed at different temperatures in order to determine different phase structures using 2D WAXD experiments. The samples used in PLM observations were melt-pressed between two glass slides with a typical gap thickness of 10 μm. Thin film samples prepared for TEM via solution casting from a 0.05% (w/v) chloroform solution on to carbon-coated mica had a thickness of 50−150 nm. After crystallization, the films were floated onto the water surface and recovered using the TEM copper grids.

Equipment and Experiments. The thermal behaviors of the phase transitions were studied using a Perkin-Elmer PYRIS Diamond DSC with an Intracooler 2P apparatus. The temperatures and heat flows were calibrated using material standards at cooling and heating rates ranging from 2.5 to 40 °C/min. The heating experiments always preceded the cooling experiments in order to eliminate previous thermal histories, and the cooling and heating rates were always kept identical. The transition temperatures were determined by measuring the onset and peak temperatures from both the cooling and heating scans at different rates. An onset temperature was defined by the cross-point of the peak slope and the baseline in the DSC trace. During cooling, the onset temperature was

determined on the high-temperature side, and upon heating the onset temperature was determined on the low-temperature side.

Phase structures and transformations were identified using 1D WAXD powder experiments. These were conducted in the transmission mode of a Rigaku 12 kW rotating-anode X-ray (Cu Kα radiation) generator coupled to a diffractometer. The diffraction peak positions and widths were calibrated with silicon crystals of known crystal size in the high 2θ angle region (>15°) and silver behenate in the low 2θ angle region. A hot stage was coupled to the diffractometer in order to study the LC structural evolutions with temperature changes during cooling and heating. The temperature of this hot stage was calibrated to be within an accuracy of ±1 °C. Samples were scanned between 1.5° and 35° at a scanning rate of 4°/min. The oriented fiber 2D WAXD patterns were obtained using a Rigaku X-ray imaging system with an 18 kW rotating anode X-ray generator. A hot stage was also used to obtain diffraction patterns from the crystal and LC structures at different temperatures. The patterns were recorded on an image plate (Rigaku, R-AXIS-IV). A 30 min exposure time was required for a high-quality pattern. In both 1D and 2D WAXD experiments, background scattering was subtracted from the sample scans.

TEM (FEI Tacnai 12) experiments were carried out to examine crystal morphology on the nanometer scale using an accelerating voltage of 120 kV. SAED patterns of the sample having different zones were also obtained using a tilting stage to determine the crystal unit cell symmetry and dimensions. The camera length was set at 2.1 m, and calibration of the SAED spacing smaller than 0.384 nm was carried out using evaporated thallous chloride, which has a largest first-order spacing diffraction of 0.384 nm. Spacing values larger than 0.384 nm were calibrated by doubling the d spacing values of the first-order diffractions. Morphological observation of the phases on the micrometer scale at different temperatures was conducted on an Olympus (BH-2) PLM coupled with a Mettler heating stage (FP-90).

Crystallographic simulation was performed using Cerius^2 (Version 4.6) simulation software from Accelrys utilizing the COMPASS force field. The lowest energy conformation of the single polymer chain was chosen as the starting conformation. Basic unit cell parameters determined by crystallographic experimental data from 2D WAXD and SAED experiments were used in order to build the crystal unit cell. The positions of atoms in this unit cell were judged by comparing their calculated diffraction patterns with those of experiments.

Results and Discussion

Thermodynamic Transitions and Their Corresponding Structural Evolutions. Figure 1a shows a set of DSC cooling and subsequent heating thermal diagrams for asymmetric bent main-chain BPE-Cn (n = 6, 8, and 10) at a rate of 2.5 °C/min. Three transition processes are observed during cooling. In the case of BPE-C6, a broad high-temperature exothermic process can be deconvoluted into two exothermic peaks at 200 and 196 °C, which can also be verified by 1D WAXD results at these temperatures. For BPE-C8, the three transition processes are observed at 188, 180, and 148 °C. In the case of BPE-C10, three transition processes take place at 162, 157, and 94 °C, respectively. It is evident that the BPE-Cn samples containing the longer methylene spacers exhibit lower transition temperatures, which is often observed in main-chain LC polymers. These three transition processes are also detected during heating at the same rate, but the transitions overlap.

Figure 1b shows two sets of DSC cooling and subsequent heating thermal diagrams for BPE-C8 at different rates ranging from 2.5 to 40 °C/min, as an example for the three BPE-Cn samples. The heats of transition for

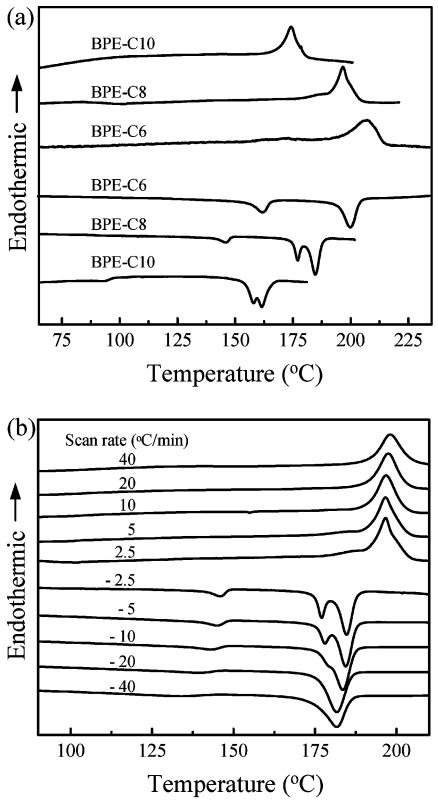

Figure 1. Sets of DSC cooling and subsequent heating thermal diagrams for BPE-Cn (n = 6, 8, and 10) samples at a rate of 2.5 °C/min (a) and for BPE-C8 at cooling and heating rates ranging from 2.5 to 40 °C/min (b).

the two high-temperature transitions measured during cooling are 3.36 kJ/mol at 188 °C and 6.47 kJ/mol at 180 °C. These two heats of transitions and the onset transition temperatures at the high-temperature side do not exhibit cooling rate dependence, although these two transition peak widths become broadened with increased cooling rate. This indicates that these two high-temperature transitions take place close to thermodynamic equilibrium, and they may be associated with the transitions between an isotropic melt (I) and a LC phase and between two LC phases.[43−46] In contrast, the heat of transition (2.17 kJ/mol) at the lowest transition temperature (148 °C, measured at 2.5 °C/min) is cooling rate dependent. Furthermore, if we compare the cooling diagram with the heating diagram in Figure 1b, it is clear that the lowest transition process possesses a large undercooling; i.e., the melting endotherm is over 30 °C higher than the exotherm during cooling, commonly indicating a crystallization process.

Although DSC experiments are sensitive to heat absorption and release events, this technique cannot provide direct information about structural changes and molecular interactions. Therefore, 1D WAXD experiments at different temperatures are utilized to identify the corresponding structural evolutions.

Figure 2a shows a set of 1D WAXD powder patterns during cooling at different temperatures (at a rate of 2.5 °C/min) for BPE-C8. In this figure, structures with two different length scales can be identified. One is on the nanometer scale in the low 2θ angle region between 1.5° and 9°, and another on the subnanometer scale can be identified between 9° and 35°. The 1D WAXD power patterns in Figure 2a show three phase transitions, and they agree with the observations in the DSC cooling

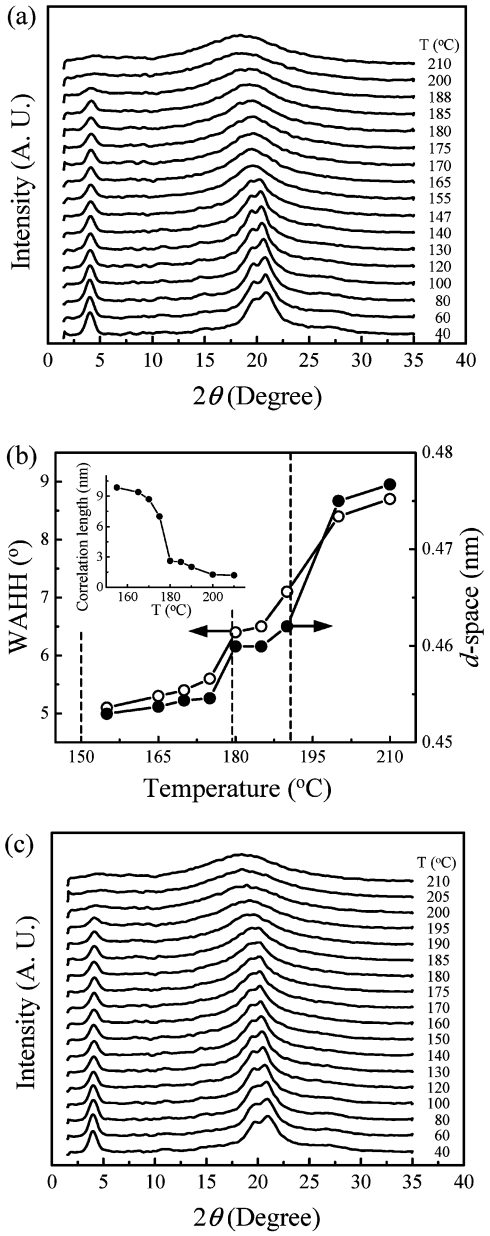

Figure 2. Set of 1D WAXD powder patterns of BPE-C8 during cooling at a rate of 2.5 °C/min at different temperatures (a). The relationship of the *d* spacings of the center scattering halos and correlation lengths of these scattering halos of BPE-C8 for temperatures above the crystallization temperature (b). The correlation lengths were calculated on the basis of the Scherrer equation. The vertical dashed lines are indications of the thermal transitions based on the DSC cooling rate. Set of 1D WAXD powder patterns of BPE-C8 during heating at a rate of 2.5 °C/min at different temperatures (c).

diagrams (Figure 1b). At temperatures above 188 °C, BPE-C8 is in the I phase. Only an amorphous halo at $2\theta = 18.6°$ (d spacing = 0.477 nm) is observed. This corresponds to a liquidlike, short-range order in the lateral molecular packing. Its correlation length is estimated to be about 1.2 nm by the Scherrer equation.[43−48] When the temperature reached 188 °C, a low-angle diffraction at $2\theta = 4.05°$ (d = 2.18 nm) starts to develop, and this usually indicates the formation of the layer structure of a smectic LC phase. The temperature where the diffraction at $2\theta = 4.05°$ appeared also corresponds to a sudden narrowing of the high 2θ angle scattering halo with a shift of the 2θ angle from 18.6° to 19.3° (d spacing from 0.477 to 0.460 nm). At 180 °C, a slight narrowing of this scattering halo with a sudden shift of 2θ angle to 19.6° (d = 0.453 nm) takes place, and they correspond to an exothermic process at the same temperature in Figure 1b. Finally, sharp reflections develop in the high 2θ angle region below 148 °C, and the reflection peak in the low 2θ angle region is also enhanced as shown in Figure 2a.

The structural changes of BPE-C8 in Figure 2a can be characterized by the d spacing changes and changes in the width at half-height (WAHH) of the high 2θ angle scattering halo with respect to temperature above the crystallization temperature of 148 °C. The correlation lengths of this halo can be calculated using the WAHH data based on the Scherrer equation. The results are shown in Figure 2b. The vertical dashed lines are indications of the thermal transitions based on the DSC cooling results. The changes in these structural parameters correspond well to the thermal transitions observed in DSC. The 1D WAXD powder patterns during heating at 2.5 °C/min (Figure 2c) are less obvious to observe the structure changes compared with those during cooling since the crystal melting takes place at a higher temperature (∼180 °C). However, they agree with the thermal transitions observed in the DSC heating results (Figure 1b).

Identification of Crystal Structures. To determine the structural symmetry and lattice parameters, 2D WAXD experiments on oriented BPE-C*n* samples are conducted. A 2D WAXD pattern for BPE-C8, from a fiber drawn in the LC phase at 185 °C and annealed at 145 °C for 1 day, is shown in Figure 3a. This pattern exhibits diffractions not only on the equator and meridian but also in the quadrants. As indicated in this figure, the a^* and b^* axes are assigned to the equator, and the c^* axis is along the fiber drawn (FD) direction. On the equator of this fiber pattern, only one strong diffraction spot appears at $2\theta = 21.1°$ (d = 0.42 nm). When the diffraction spots in the quadrant are projected onto the equator, the locations of these four extinct diffraction spots on the equator can be identified at $2\theta = 10.5°$ (d = 0.84 nm), 14.9° (d = 0.60 nm), 18.2° (d = 0.49 nm), and 25.9° (d = 0.34 nm). They can be assigned to be the (010), (100), (110), and (120), respectively, based on the triangulation method of building a 2D a^*b^* lattice of the unit cell.[49] The strong diffraction spot observed at $2\theta = 21.1°$ is assigned to be the (020). On the basis of these diffraction spots on the equator, the γ angle is calculated to be 90°. On the meridian of this fiber pattern, there are four diffraction spots at $2\theta = 3.90°$ (d = 2.27 nm), 7.80° (d = 1.13 nm), 11.7° (d = 0.75 nm), and 15.6° (d = 0.57 nm), respectively, and they should be assigned as the (002) and its higher order (004), (006), and (008) diffractions. This assignment is based on two facts. First, the bend at the end of the mesogen of BPE-C8 is an asymmetric chemical repeat unit; therefore, two repeat units of each BPE-C8 chain must be involved to construct the minimum structural repeat unit of this unit cell. Second, the diffraction spots (hkl) in the quadrants of the fiber pattern with l = odd numbers can be observed in between the neighboring (00l) (l = even numbers) diffractions. Careful structural analysis gives an orthorhombic unit cell with dimensions of a = 0.60 nm, b = 0.84 nm, c = 4.53 nm, and $\alpha = \beta = \gamma = 90°$ via the refinement of the reciprocal lattice using a procedure developed in our laboratory, and this phase is abbreviated to be the K_O phase. Table 1 lists the experimentally observed and the calculated 2θ values

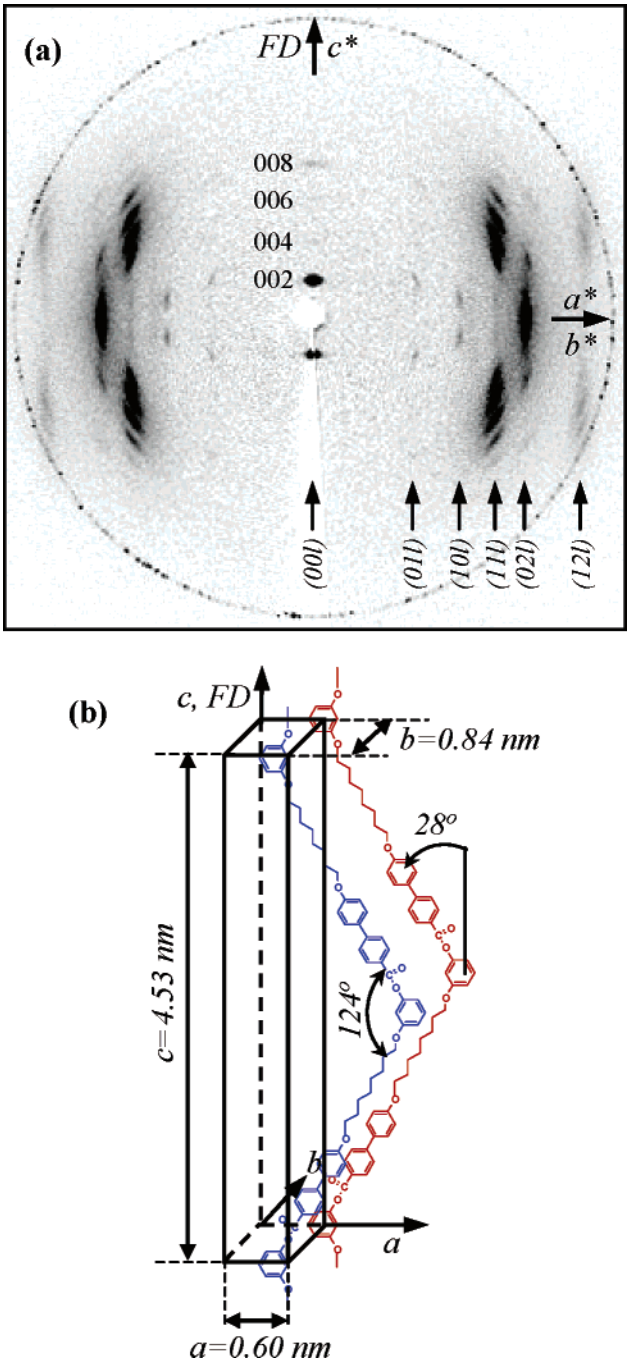

Figure 3. 2D WAXD fiber pattern of the K_O crystalline phase of BPE-C8 after the sample was annealed at 145 °C for 1 day (a). The fiber draw direction and c^* axis is along the meridian direction while the a^* and b^* axes are along the equatorial direction. A schematic unit cell model with two chains for the K_O crystalline phase of BPE-C8 (b).

and the d spacings based on this unit cell lattice. With two chains (four chemical repeating units) in this orthorhombic unit cell, its calculated crystallographic density is 1.23 g/cm^3. The experimentally observed density is 1.21 g/cm^3, which fits well with the calculated data.

A schematic two-chain unit cell model for this K_O crystalline phase of BPE-C8 is shown in Figure 3b. The d spacing of the (002) diffraction is 2.27 nm, while the calculated length of the chemical repeating unit is 2.57 nm. This repeat unit should thus be tilted ±28° with respect to the c axis (the FD direction) toward the a axis. The molecular tilting angle can also be measured from

Table 1. Experimental and Calculated Crystallographic Parameters of the K_O Crystalline Phase of BPE-C8

	2θ (deg)		d-spacing (nm)		
hkl	expt[a]	calcd[b]	expt[a]	calcd[b]	int[c]
020	21.1	21.1	0.42	0.42	vs
011	10.7	10.7	0.83	0.83	vw
101	15.0	15.0	0.59	0.59	m
111	18.3	18.3	0.48	0.48	w
002	3.90	3.90	2.27	2.27	vs
012	11.2	11.2	0.79	0.79	m
022	21.4	21.4	0.42	0.41	m
023	21.9	21.9	0.40	0.41	s
113	19.2	19.2	0.46	0.46	vs
123	26.6	26.6	0.34	0.34	w
004	7.80	7.80	1.13	1.13	m
014	13.1	13.1	0.68	0.68	w
114	19.9	19.9	0.45	0.45	vs
124	27.1	27.1	0.33	0.33	s
015	14.4	14.3	0.62	0.62	w
115	20.7	20.7	0.43	0.43	vs
125	27.7	27.7	0.32	0.32	m
006	11.7	11.7	0.75	0.76	m
016	15.8	15.8	0.56	0.56	w
116	21.7	21.7	0.41	0.41	s

[a] The accuracy of the experimental data is ±0.005 nm. [b] The calculated data listed are based on the K_O orthorhombic unit cell with a = 0.60 nm, b = 0.84 nm, c = 4.53 nm, and $\alpha = \beta = \gamma$ = 90.0°. [c] The intensities are semiquantitatively estimated via a microdesitometer and classified as very strong (vs), strong (s), medium (m), weak (w), and very weak (vw).

the strongest (114) diffraction spot among the set of (11l) diffraction spots. The measured tilting angle is 28°, which is identical to the calculated value. Therefore, the bending angle at the center of the structural repeating unit (the center of two chemical repeating units) is 124°. Since the only experimentally observed diffraction on the equator is the (020), the two zigzag chains must lie more or less on the (0k0) plane.

This structural determination and schematic two-chain unit cell model for the K_O phase in BPE-C8 can be supported by SAED experiments conducted on BPE-C8 single crystals in TEM. Figure 4a shows a stack of lamellar crystals grown at a cooling rate of 0.1 °C/min from the I phase and annealed at 145 °C for 12 h under a dry nitrogen atmosphere. The lamellae appear to be edge-on. The [010] zone SAED pattern is obtained from this lamellar stack of the K_O phase when the sample is not tilted, as shown in Figure 4b. In this SAED pattern, it is evident that no diffractions can be observed on the a^* axis due to the reason that all the (hk0) diffractions are extinct (as shown in the 2D WAXD fiber pattern in Figure 3a), except for the (020) diffraction. However, the (020) diffraction cannot be seen in this SAED pattern since the b^* axis is perpendicular to the a^*c^* plane. The observation of the (101) ED spot confirms that the (00l) (l = odd numbers) are extinct in the 2D WAXD fiber pattern, and the diffraction spots on the meridian must be assigned as the (002), (004), (006), and (008). The (100) ED spot is also extinct in this ED pattern, as observed in the case of the 2D WAXD fiber pattern. To obtain an ED pattern from the [001] zone, which provides the packing symmetry in the unit cell, the BPE-C8 sample in the I phase was quenched to room temperature and annealed at 145 °C for 12 h (the inset of Figure 4c). A SAED pattern from the [001] zone can be observed and is shown in Figure 4c. Only the (020) and (040) ED spots are observed as seen in the X-ray diffractions on the equator of the 2D WAXD fiber pattern (Figure 3a). The symmetry group of the K_O phase was determined to be $Pna2_1$ on the basis of the SAED results.

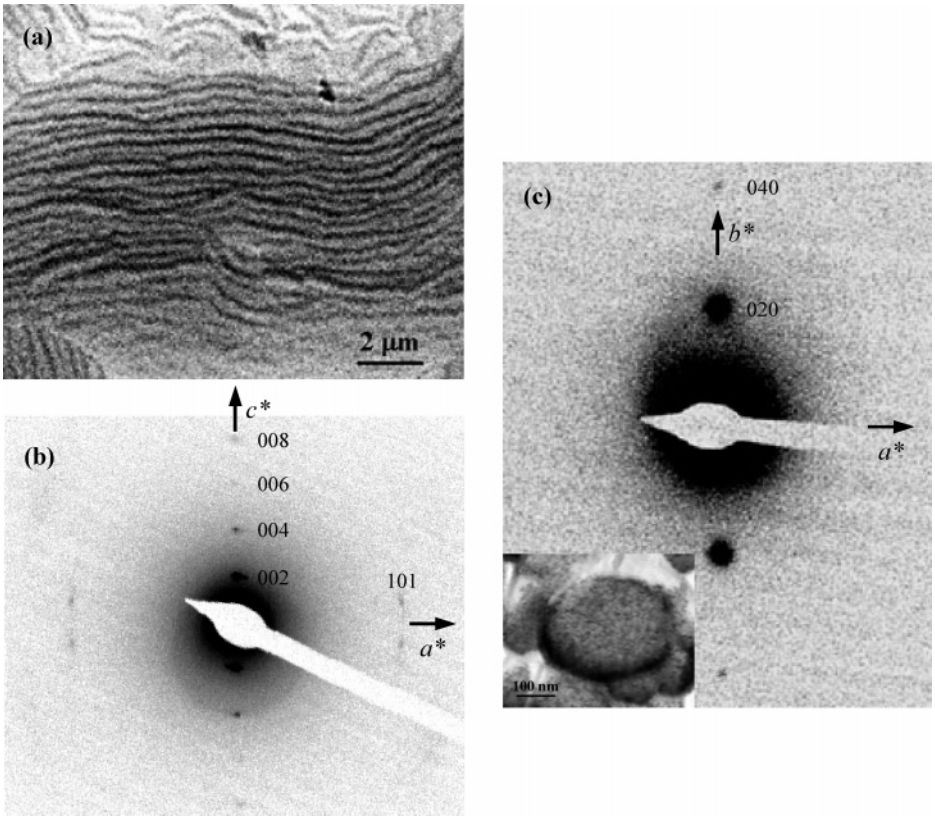

Figure 4. TEM morphology (a) and SAED pattern of the [010] zone (b) without tilting for the edge-on lamellar crystals of BPE-C8. SAED pattern of the [001] zone for the K_O phase of BPE-C8 (c). The inset of (c) is the TEM morphology of the [001] zone SAED pattern.

Table 2. Crystal System, Axial System, and Density of the K_O Phase of BPE-C*n* at Room Temperature

		axial system						density	
n	crystal system	*a* (nm)	*b* (nm)	*c* (nm)	α (deg)	*β* (deg)	*γ* (deg)	expt	calcd
6	orthorhombic	0.61	0.83	4.02	90.0	90.0	90.0	1.25	1.27
8	orthorhombic	0.61	0.84	4.53	90.0	90.0	90.0	1.21	1.23
10	orthorhombic	0.62	0.85	4.75	90.0	90.0	90.0	1.16	1.18

Confirmation of this structure determination and the detailed positions of atoms in the K_O two-chain (four chemical repeating units) unit cell of BPE-C8 with a symmetry group of $Pna2_1$ can be provided via computer calculations. These calculations can generate a detailed chain-packing scheme. To examine whether this proposed packing scheme fits to the real structure, the calculated diffraction patterns are generated and compared with the experimentally obtained diffraction patterns. First, the global equilibrium conformation of the monomer BPCA-C8-P*m*OH was constructed at 0 K using the COMPASS force field. The energy-minimized monomers were used to construct the BPE-C8 polyester. The lowest energy conformation of the single polymer chain was chosen as the starting conformation. To build the K_O structure with two polymer chains using $Pna2_1$ symmetry, basic unit cell parameters determined by experimental data from 2D WAXD and SAED experiments were used. Figure 5a shows the two-chain packing scheme suggested by the computer calculations from the side (the [100] zone, Figure 5b) and top (the [001] zone, Figure 5c) views. The calculated 2D WAXD fiber patterns and SAED pattern with the [001] zone based on this scheme are shown in parts d and e of Figure 5, respectively. Both (Figures 5d and 5e) qualitatively match with the experimental observations (Figures 3a and 4c, respectively).

For the other two polymers BPE-C*n* (n = 6 and 10), their 2D WAXD fiber patterns are shown in parts a and b of Figure 6, respectively. It is evident that these two patterns are similar to that of the BPE-C8 as shown in Figure 3a. Detailed structural determinations of these two crystal structures lead to the identical orthorhombic lattice and symmetry of the BPE-C8 crystal structures. Their lattice, unit cell dimensions, and density data are listed in Table 2. As shown in this table, with an increasing the number of methylene units, the unit cell dimensions increase, while the densities decrease.

Identification of Liquid Crystal Structures. A 2D WAXD for an oriented BPE-C8 fiber sample, drawn in the LC phase and annealed at 175 °C for 10 h under a dry nitrogen atmosphere, is shown in Figure 7a. Compared with the 2D WAXD fiber pattern of the K_O phase in Figure 3a, this figure shows fewer and diffused diffraction spots on the meridian and in the quadrants, but the overall diffraction pattern does not exhibit any substantial changes. At first, Figure 7a appears to show a highly ordered smectic crystal phase based on our previous publications.[43,44] Therefore, chain conformations and packing scheme in this highly ordered smectic LC phase should not be very different from those in the K_O phase.

When we start to determine the structural lattice, difficulty immediately arises due to the large zigzag

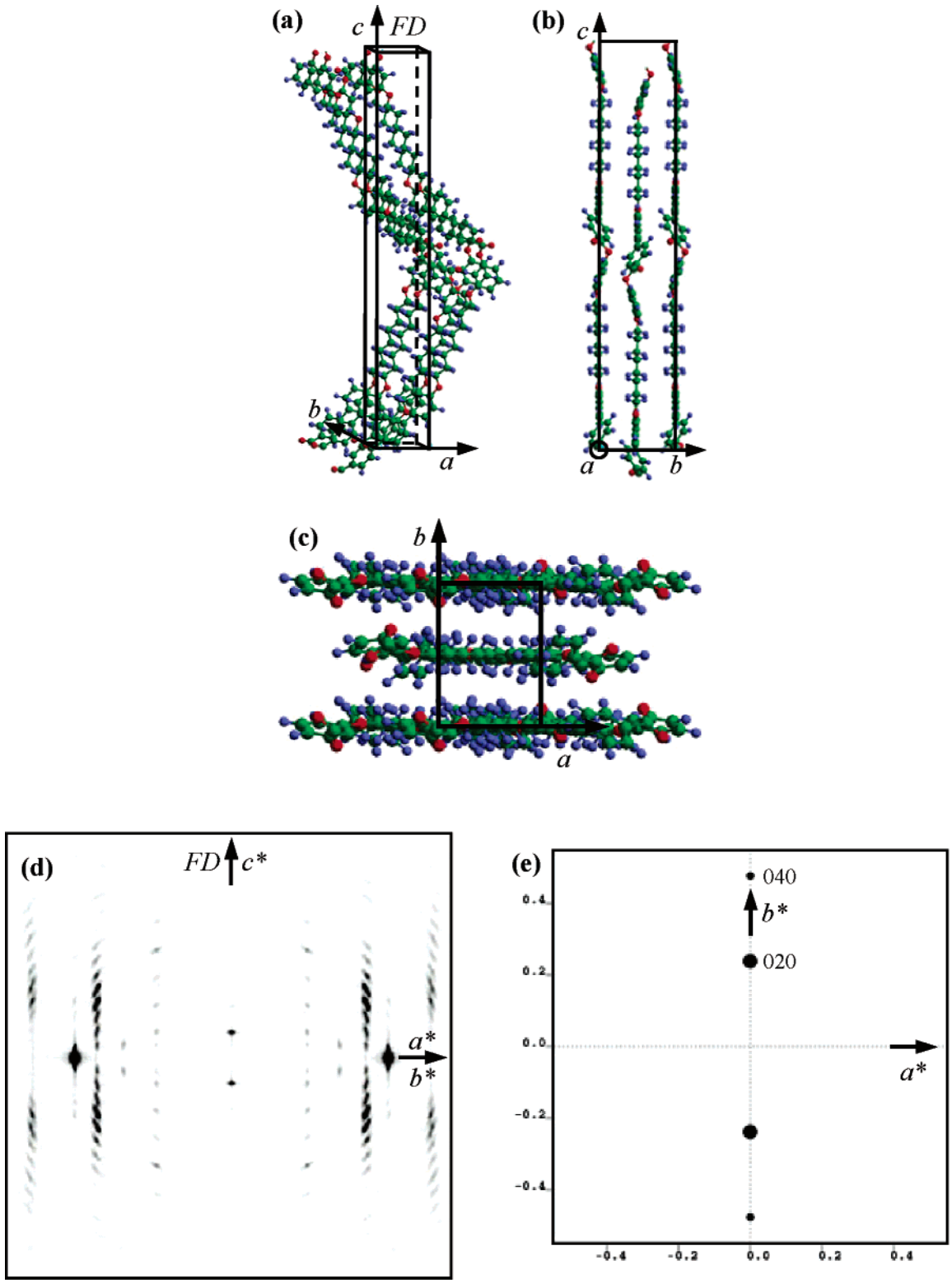

Figure 5. Computer simulated BPE-C8 chain packing scheme in unit cell with the best match to the experimental 2D WAXD and SAED patterns (a) with views from the side ([100]-zone) (b) and the top ([001]-zone) views (c). Computer calculated 2D WAXD pattern (d) and SAED pattern of the [001] zone (e), which agree well with those of the experimental 2D WAXD (Figure 3a) and SAED (Figure 4c) diffraction patterns.

chain conformation and its packing scheme. It is evident that in this structure the chemical repeating units form layers perpendicular to the FD direction, and the neighboring layers are anticlinically tilted by ±31.5° with respect to FD direction (as described in Figure 7b). Within each individual layer, the repeat units are synclinically oriented. If we view each chemical repeat unit layer as the structural block, a monoclinic lattice can be determined with $a = 1.05$ nm, $b = 0.50$ nm, $c = 2.21$ nm, $\alpha = 90.0°$, $\beta = 58.5°$, and $\gamma = 90.0°$. Along the long axis of the chemical repeating unit, a 2D rectangular lattice can be observed.

From the crystallographic point of view, however, one smectic crystal repeating unit must include two neighboring chemical repeating unit layers along the chain direction because of the symmetry requirement of the

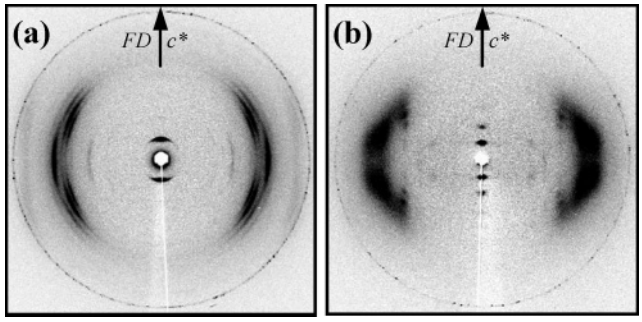

Figure 6. 2D WAXD fiber pattern of the K_O crystalline phase of BPE-C6 (a) and BPE-C10 (b) after the sample was annealed for 1 day at 150 and 85 °C, respectively.

Table 3. Experimental and Calculated Crystallographic Parameters of the Highly Ordered Smectic Crystal Phase of BPE-C8

	2θ (deg)		d-spacing (nm)		
hkl	expt[a]	calcd[b]	expt[a]	calcd[b]	int[c]
002	4.00	4.00	2.21	2.21	vs
023	20.4	20.4	0.43	0.43	vs
004	8.01	8.00	1.10	1.11	w
114	18.9	18.9	0.47	0.47	s
115	19.9	19.9	0.45	0.45	vs
116	21.0	21.0	0.42	0.42	m

[a] The accuracy of the experimental data is ±0.005 nm. [b] The calculated data listed are based on the orthorhombic unit cell with $a = 0.63$ nm, $b = 0.91$ nm, $c = 4.42$ nm, and $\alpha = \beta = \gamma = 90.0°$. [c] The intensities are semiquantitatively estimated via a microdesitometer and classified as very strong (vs), strong (s), medium (m), weak (w), and very weak (vw).

structural repeat unit, as illustrated in Figure 7b. Similar to the K_O crystal phase case of BPE-C8, the a^* and b^* axes can still be assigned to the equator and the c^* axis is along the FD direction (Figure 7a). On the equator of this fiber pattern, the (020) diffraction spot is not seen possibly due to disordered arrangements of the zigzag chains. When the diffraction spots in the quadrant are projected onto the equator, extinct diffraction spots on the equator can be found at $2\theta = 17.1°$ ($d = 0.518$ nm) and 19.5° ($d = 0.455$ nm), which can be assigned to be the (110) and (020), respectively. On the meridian of this fiber pattern, a pair of strong diffraction spots are at $2\theta = 4.00°$ ($d = 2.21$ nm) with a higher order weak diffraction at $2\theta = 8.01°$ ($d = 1.10$ nm). Again, they are assigned to the (002) and (004), respectively, indicating that the structural repeat unit consists of two chemical repeat units of BPE-C8 in this highly ordered smectic crystal phase. The two strongest pairs of scattering spots in Figure 7a are at $2\theta = 20.5°$ ($d = 0.43$ nm), which is attributed to the lateral packing of the molecules, and possess a correlation length of ~10 nm as estimated by the Scherrer equation. Careful structural analysis gives rise to an orthorhombic unit cell with dimensions of $a = 0.63$ nm, $b = 0.91$ nm, $c = 4.42$ nm, and $\alpha = \beta = \gamma = 90°$ via the refinement. Therefore, this highly ordered smectic crystal phase should be an anticlinically tilted SmH (SmH_A) phase. Table 3 lists the experimentally observed and calculated 2θ angles and d spacings based on this unit cell lattice. With two chains (four chemical repeating units) in this orthorhombic unit cell, its calculated crystallographic density is 1.20 g/cm^3.

Parts a and b of Figure 8 are two 2D WAXD fiber patterns for BPE-C6 and BPE-C10 in the highly ordered smectic crystal phases. The structures and lattices are identical to that of BPE-C8 from the crystallographic

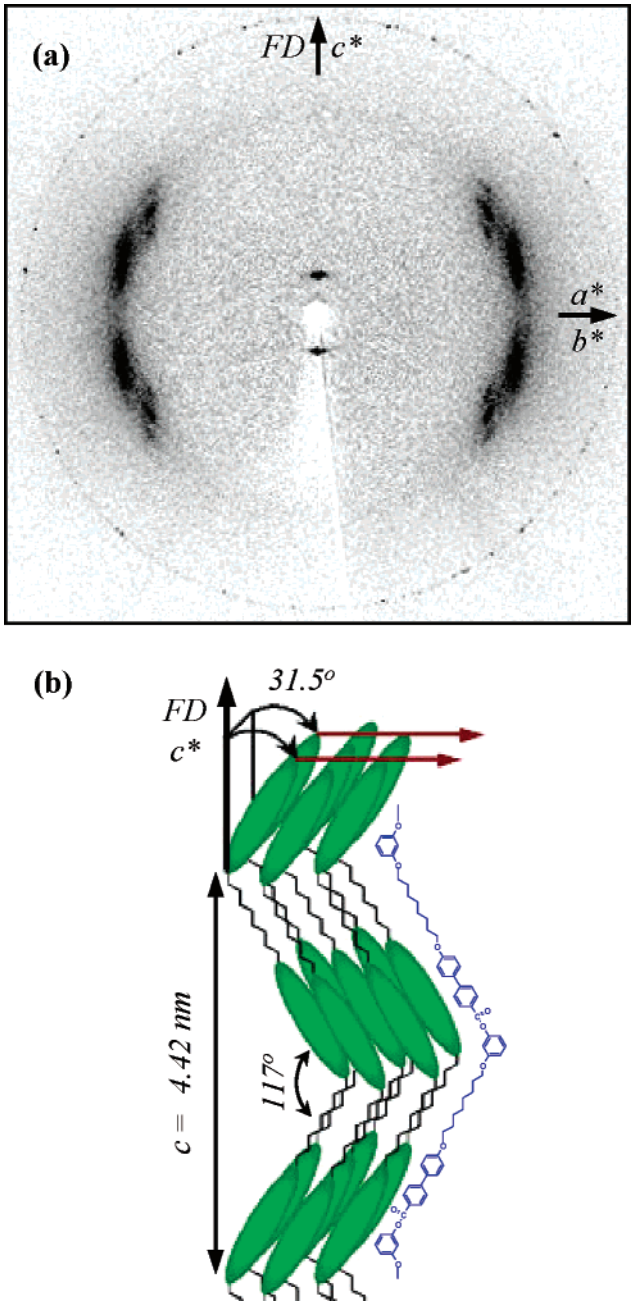

Figure 7. 2D WAXD fiber pattern of the highly ordered smectic crystal phase of BPE-C8 after the sample was annealed at 175 °C for 10 h (a). The fiber draw direction and c^* axis are along the meridian direction while the a^* and b^* axes are along the equatorial direction. A schematic chain-packing model for the highly ordered smectic crystal phase of BPE-C8 (b).

point of view, yet the dimensions increase with an increasing number of methylene units. All of the structural parameters, based on experimentally observed and calculated data, for these three polyesters in the highly ordered smectic crystal phase are listed in Table 4.

The structure of the LC phase observed between 180 and 188 °C can also be identified using the 2D WAXD fiber pattern from BPE-C8. The fiber samples were obtained by annealing the fiber at 185 °C for 2 h under a dry nitrogen atmosphere, and the resultant WAXD pattern is shown in Figure 9a. In the high 2θ angle region, two pairs of scattering halos at $2\theta = 19.3°$ ($d = 0.46$ nm) in the quadrants (±20° away of the equator) represent a liquidlike lateral short-range ordering within

Table 4. Crystal System, Axial System, and Density of BPE-C*n* in the Highly Ordered Smectic Crystalline Phase

		axial system						density
n	crystal system	*a* (nm)	*b* (nm)	*c* (nm)	α (deg)	*β* (deg)	*γ* (deg)	calcd
6	orthorhombic	0.61	0.90	4.02	90.0	90.0	90.0	1.25
8	orthorhombic	0.63	0.91	4.42	90.0	90.0	90.0	1.20
10	orthorhombic	0.64	0.93	4.70	90.0	90.0	90.0	1.15

the layer. Their correlation lengths are ~2.5 nm, as estimated by the Scherrer equation. This illustrates that the mesogens possess ±20° chain tilting with respect to the layer normal (the FD direction), as shown in Figure 9b. A pair of low 2θ angle diffraction spots on the meridian appear at 2θ = 4.05° (d = 2.18 nm), indicating that the layer normal is along the FD direction. It is predicted that the chain orientation in the drawn polymer sample in this low ordered LC phase does not significantly change during the transition from the highly ordered smectic crystal phase. Within each chemical repeating unit layer, the chain orientation is synclinic. However, two neighboring layers construct one smectic layer structure (the diffraction on the meridian), and the alternated neighboring layers construct an anticlinically tilted SmC (SmC_A) phase,[13−20,48] as illustrated in Figure 9b. The bending angle of the BPE-C8 zigzag conformation in this SmC_A phase is ~140°. On the basis of the tilting angle (±20°) and the measured layer thickness (2.18 nm), the length of a chain in one layer of this SmC_A phase is calculated to be 2.32 nm, which is shorter than the calculated length of the chain (2.56 nm). This difference may be due to the fact that the alkoxyl chains of BPE-C8 in this SmC_A phase contain gauche and trans conformations instead of the assumed all-trans conformation in the calculation.[11,50−54] The 2D WAXD fiber patterns of the other two BPE-C*n* samples (n = 6 and 10) are shown in Figure 10a,b, and they are also identified as SmC_A phases. The layer diffractions of these SmC_A phases for BPE-C6 and BPE-C10 are at 2θ = 4.39° (d = 2.01 nm) and 2θ = 3.70° (d = 2.39 nm), respectively.

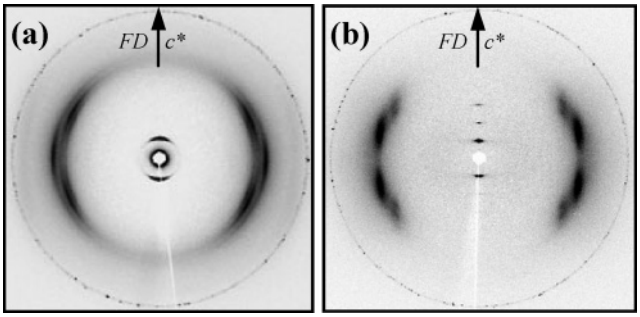

Figure 8. 2D WAXD fiber pattern of the highly ordered smectic crystal phase of BPE-C6 (a) and BPE-C10 (b) after the sample was annealed for 10 h at 175 and 145 °C, respectively.

One issue still remains: Figures 9 and 10 do not warrant the SmC_A chain packing, since this 2D WAXD pattern can also be constructed by a mixture of two (conventional) SmC_S domains with opposite chain tilting directions. However, the argument can be made that the chain conformation in the K_O phase and SmH_A phase is zigzag type, and the c axes of the unit cells are identified to include two chemical repeat units. If the SmC_S phase were formed, the transition between the SmC_S and SmH_A phases would require a large extra volume in order to provide space for the significant change between a zigzag to a linear chain conformation.

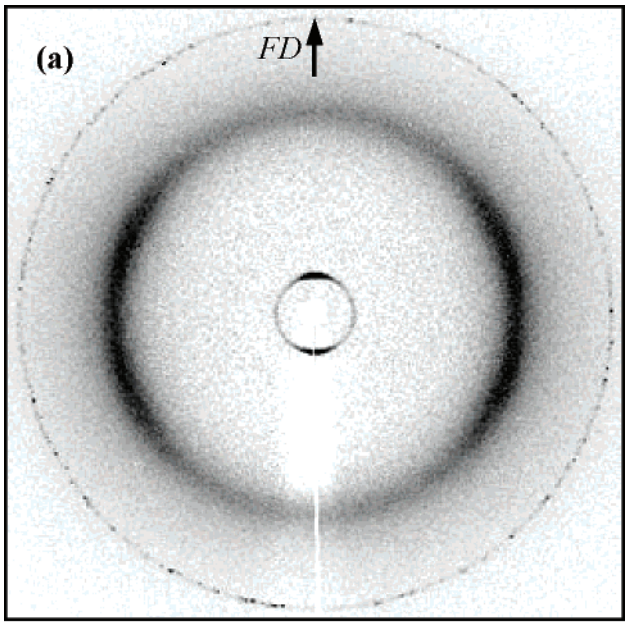

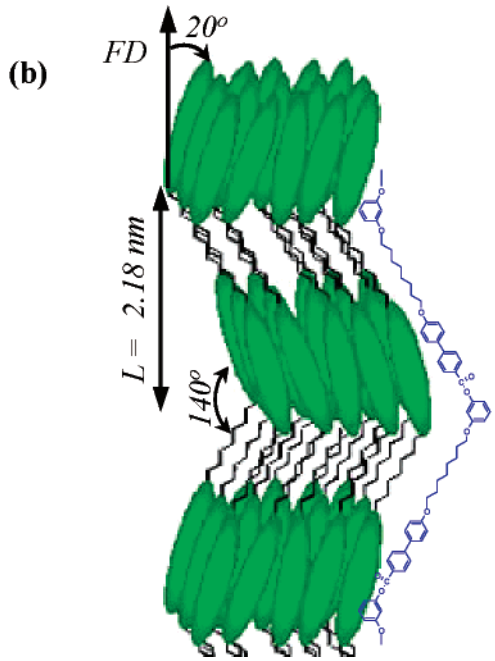

Figure 9. 2D WAXD fiber pattern of the low-ordered SmC_A LC phase of BPE-C8 after the sample was annealed at 185 °C for 2 h (a). The fiber draw direction is along the meridian. A schematic chain-packing model for the SmC_A LC phase of BPE-C8 (b).

Both the free volume creation and conformation changes would take an enormous amount of energy. Therefore, the most probable chain conformation in the SmC phase must retain the zigzag to form the SmC_A phase.

Liquid Crystalline Textures. The phase identifications of BPE-C*n* polyesters based on diffraction methods can also be supported by the observation of texture changes in PLM at the transitions. Figure 11a−c shows

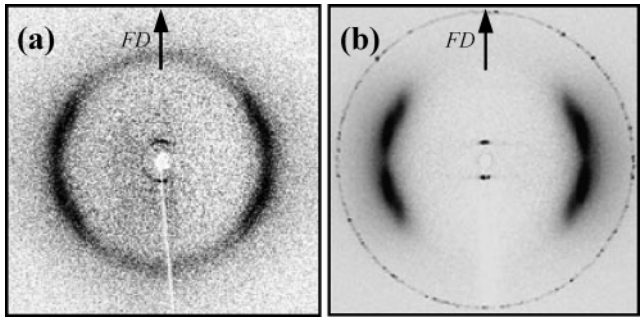

Figure 10. 2D WAXD fiber pattern of the low-ordered SmC_A LC phase of BPE-C6 (a) and BPE-C10 (b) after the sample was annealed for 2 h at 198 and 160 °C, respectively.

changes in the BPE-C8 morphological textures upon cooling. At the cooling rate of 0.1 °C/min, the transition from the I melt to the SmC_A phase occurs at 188 °C. At this point a bâtonnet-like texture having cauliflower-shaped domains against the I melt can be observed (Figure 11a).[55,56] When the temperature reaches 180 °C, a fan-shaped texture with spherulitic domains appears as shown in Figure 11b, which is often observed in smectic phases.[55] At a lower temperature deep into the highly ordered smectic crystal phase, concentric rings start to develop. By further decreasing the temperature below the exothermic process at 148 °C, a pronounced ring striation, a nonequidistant arc pattern, can be observed as shown in Figure 11c. The rings show three different colors: green, yellow, and brown, which may correspond to the three orientations of the orthorhombic structure.[55] The rotation would occur along the normal direction of the ring striations. A detailed quantitative investigation is currently underway.

Figure 12a shows a cluster of oriented bâtonnet-like textures induced by mechanical shearing of the sample in the SmC_A phase, similar to the observations previously reported.[56] The chain orientation is parallel to the shear direction. When this sample is annealed more than 10 h in the SmC_A phase under a dry nitrogen atmosphere, bigger elongated bâtonnet-like texture domains appear. In the SmC_A phase of this series of BPE-C*n*, no helical supramolecular texture can be observed even though the bending angle of BPE-C*n* polymer chain is ~140°, which is similar to that of banana-shaped LC small compounds.[30−34] This is because the BPE-C*n* are polymers, so the chemical repeating units are connected by covalent bonds. The strong chemical bonding allows the retention of the zigzag conformation but does not permit continuous twisting of the chemical repeat unit from one to another along the same twisting direction as in the case of their corresponding monomers.[41] Additionally, in BPCA-C*n*-P*m*OH, the chemical repeat units are connected in a head-to-head sequence,[41] while in the BPE-C*n* polymers, it is a covalent head-to-tail connection. On the other hand, the ring striation, observed in PLM, shows three different colors which may be an indication of limited crystal twisting on the micrometer length scale.

Conclusion

A series of new asymmetric bent main-chain LC polyesters (BPE-C*n*) synthesized through the condensation polymerization of the A−B type asymmetric BPCA-C*n*-P*m*OH monomers containing different numbers of methylene spacers (n = 6, 8, and 10) exhibit three different phases as observed via DSC measurements.

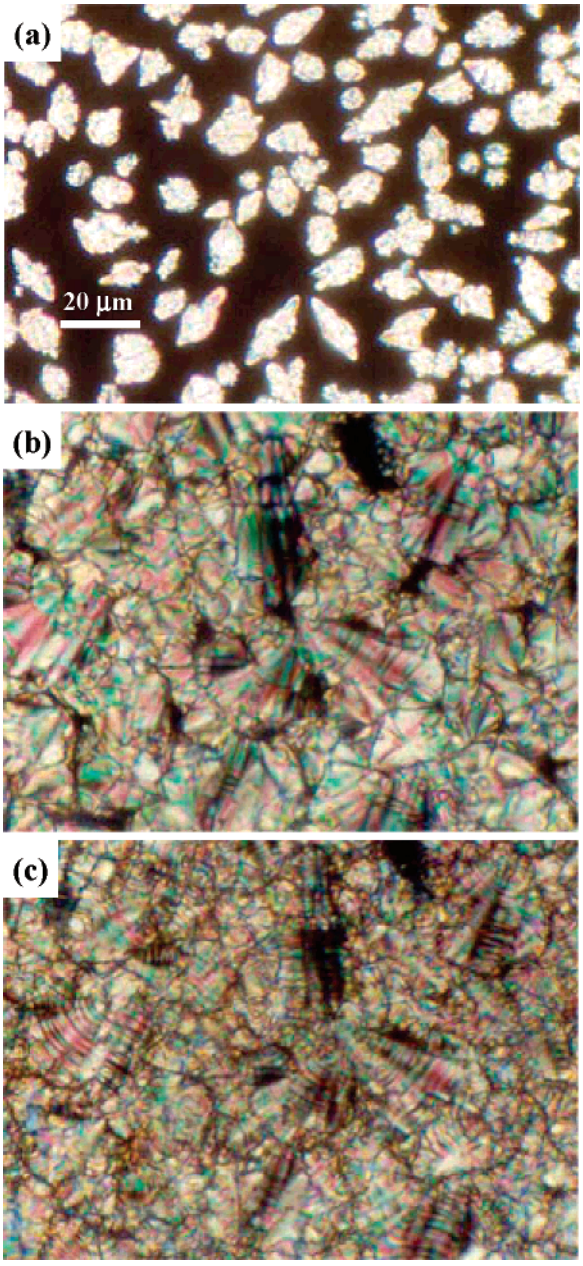

Figure 11. Morphological observations of BPE-C8 under PLM at different temperatures at a cooling rate of 0.1 °C/min: the SmC_A phase at 185 °C (a), the highly ordered smectic crystal phase at 160 °C (b), and the K_O phase at 30 °C (c).

On the basis of 2D WAXD and SAED results, these three phases are identified to be the low-ordered SmC_A phase, the highly ordered SmH_A phase, and the crystalline orthorhombic K_O phases. A detailed chain-packing scheme for the orthorhombic crystalline phase (K_O) has been proposed on the basis of the experimental diffraction patterns and qualitatively supported using simulated structural diffractions. This structural model consists of two crystallographic units in each unit cell (which contains four chemical repeating units), and its symmetry group is $Pna2_1$. Of particular interest is that in all of these ordered phases the BPE-C*n* chains retain the large zigzag conformation which becomes the basic building block of these ordered structures. This leads to a difficulty in determining the LC phases. In each chemical repeat unit layer, the highly and low ordered smectic crystals should be syclinically packed, but because of the crystallographic rule of structure sym-

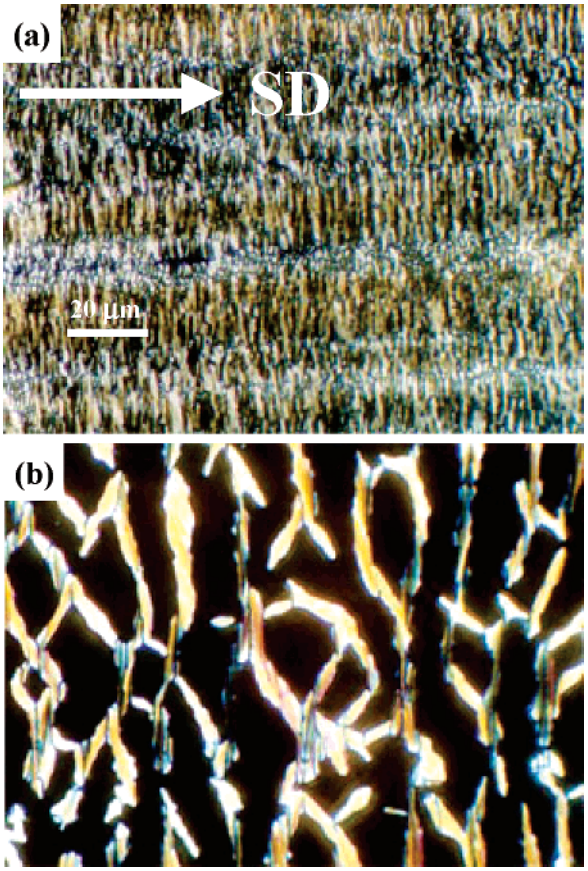

Figure 12. PLM morphological observations of the BPE-C8 sample right after mechanical shearing in the SmC_A phase (a) and the sample annealed in the SmC_A phase for 10 h (b). The arrow represents the shear direction.

metry, two neighboring layers together make the structural repeating unit to construct the SmH_A and SmC_A phases. The LC morphological transformations were also identified via PLM. Although the molecular conformation involves bends similar to the banana-shaped LC molecules, no helical supramolecular structure has been observed. This indicates that the existence of the bend in molecules is not sufficient to generate chiral characteristics. A molecular twist may also be necessary in order to achieve these characteristics, although the PLM texture does provide some indications of a possible twist in the crystal structure along the normal direction of the ring striations.

Acknowledgment. This work was supported by the National Science Foundation (DMR-0203994 and 0516602). We also acknowledge Perkin-Elmer Co. for their support in providing a Diamond DSC instrument for our laboratory.

References and Notes

(1) Greiner, A.; Schmidt, H.-W. In *Handbook of Liquid Crystals*; Demus, D., Goodby, J., Gray, G. W., Spiess, H.-W., Vill, V., Eds.; Wiley-VCH: Weinheim, 1998; Vol. 3, pp 3−25.
(2) Chiellini, E.; Laus, M. In *Handbook of Liquid Crystals*; Demus, D., Goodby, J., Gray, G. W., Spiess, H.-W., Vill, V., Eds.; Wiley-VCH: Weinheim, 1998; Vol. 3, pp 26−51.
(3) Bello, A.; Riande, E.; Pérez, E.; Marugán, M. M.; Pereña, J. M. *Macromolecules* **1993**, *26*, 1072.
(4) Orifici, A. F.; Vallés, E. M.; Garay, R. O.; Lenz, R. W. *Polymer* **1996**, *37*, 4357.
(5) Jehnichen, D.; Friedel, P.; Bergmann, J.; Taut, T.; Tobisch, J.; Pospiech, D. *Polymer* **1998**, *39*, 1095.
(6) He, C.; Lu, Z.; Zhao, L.; Chung, T.-S. *J. Polym. Sci., Part A: Polym. Chem.* **2001**, *39*, 1242.
(7) Hu, Y. S.; Liu, R. Y. F.; Schiraldi, D. A.; Hiltner, A.; Baer, E. *Macromolecules* **2004**, *37*, 2128.
(8) Ge, J. J.; Zhang, A.; McCreight, K. W.; Ho, R.-M.; Wang, S.-Y.; Jin, X.; Harris, F. W.; Cheng, S. Z. D. *Macromolecules* **1997**, *30*, 6498.
(9) Ge, J. J.; Zhang, A.; McCreight, K. W.; Wang, S.-Y.; Harris, F. W.; Cheng, S. Z. D. *Macromolecules* **1998**, *31*, 4093.
(10) Ge, J. J.; Honigfort, P. S.; Ho, R.-M.; Wang, S.-Y.; Harris, F. W.; Cheng, S. Z. D. *Macromol. Chem. Phys.* **1999**, *200*, 31.
(11) Ge, J. J.; Guo, M.; Zhang, Z.; Honigfort, P. S.; Wang, S.-Y.; Harris, F. W.; Cheng, S. Z. D. *Macromolecules* **2000**, *33*, 3983.
(12) Ruan, J.; Ge, J. J.; Zhang, A.; Jin, S.; Wang, S.-Y.; Harris, F. W.; Cheng, S. Z. D. *Macromolecules* **2002**, *35*, 736.
(13) Watanabe, J.; Hayashi, M. *Macromolecules* **1988**, *21*, 278.
(14) Watanabe, J.; Hayashi, M. *Macromolecules* **1989**, *22*, 4083.
(15) Watanabe, J.; Hayashi, M.; Morita, A.; Tokita, M. *Macromolecules* **1995**, *28*, 8073.
(16) Tokita, M.; Takahashi, T.; Hayashi, M.; Inomata, K.; Watanabe, J. *Macromolecules* **1996**, *29*, 1345.
(17) Osada, K.; Niwano, H.; Tokita, M.; Kawauchi, S.; Watanabe, J. *Macromolecules* **2000**, *33*, 7420.
(18) Tokita, M.; Tokunaga, K.; Funaoka, S.; Osada, K.; Watanabe, J. *Macromolecules* **2004**, *37*, 2527.
(19) Peterson, M. A.; Strey, H.; Sackmann, E. *J. Phys. II* **1992**, *2*, 1273.
(20) Watanabe, J.; Nakata, Y.; Simizu, K. *J. Phys. II* **1994**, *4*, 581.
(21) Li, C. Y.; Yan, D.; Cheng, S. Z. D.; Bai, F.; He, T.; Chien, L. C.; Harris, F. W.; Lotz, B. *Macromolecules* **1999**, *32*, 524.
(22) Li, C. Y.; Yan, D.; Cheng, S. Z. D.; Bai, F.; Ge, J. J.; Calhoun, B. H.; He, T.; Chien, L. C.; Harris, F. W.; Lotz, B. *Phys. Rev. B* **1999**, *60*, 12675.
(23) Li, C. Y.; Cheng, S. Z. D.; Ge, J. J.; Bai, F.; Zhang, J. Z.; Mann, I. K.; Harris, F. W.; Chien, L.-C.; Yan, D.; He, T.; Lotz, B. *Phys. Rev. Lett.* **1999**, *83*, 4558.
(24) Li, C. Y.; Ge, J. J.; Bai, F.; Zhang, J. Z.; Calhoun, B. H.; Chien, L. C.; Harris, F. W.; Lotz, B.; Cheng, S. Z. D. *Polymer* **2000**, *41*, 8953.
(25) Li, C. Y.; Cheng, S. Z. D.; Ge, J. J.; Bai, F.; Zhang, J. Z.; Mann, I. K.; Chien, L. C.; Harris, F. W.; Lotz, B. *J. Am. Chem. Soc.* **2000**, *122*, 72.
(26) Li, C. Y.; Cheng, S. Z. D.; Weng, X.; Ge, J. J.; Bai, F.; Zhang, J. Z.; Calhoun, B. H.; Harris, F. W.; Chien, L. C.; Lotz, B. *J. Am. Chem. Soc.* **2001**, *123*, 2462.
(27) Li, C. Y.; Ge, J. J.; Bai, F.; Calhoun, B. H.; Harris, F. W.; Cheng, S. Z. D.; Chien, L. C.; Lotz, B.; Keith, H. D. *Macromolecules* **2001**, *34*, 3634.
(28) Li, C. Y.; Jin, S.; Weng, X.; Ge, J. J.; Zhang, D.; Bai, F.; Harris, F. W.; Cheng, S. Z. D.; Yan, D.; He, T.; Lotz, B.; Chien, L. C. *Macromolecules* **2002**, *35*, 5475.
(29) Weng, X.; Li, C. Y.; Jin, S.; Zhang, J. J.; Zhang, D.; Harris, F. W.; Cheng, S. Z. D.; Lotz, B. *Macromolecules* **2002**, *35*, 9678.
(30) Niori, T.; Sekine, T.; Watanabe, J.; Furukawa, T.; Takezoe, H. *J. Mater. Chem.* **1996**, *6*, 1231.
(31) Link, D. R.; Natale, G.; Shao, R.; Mclennan, J. E.; Clark, N. A.; Korblova, E.; Walba, D. M. *Science* **1997**, *278*, 1924.
(32) Pelzl, G.; Diele, S.; Jákli, A.; Lischka, C.; Wirth, I.; Weissflog, W. *Liq. Cryst.* **1999**, *26*, 135.
(33) Pelzl, G.; Diele, S.; Weissflog, W. *Adv. Mater.* **1999**, *11*, 707.
(34) Thisayukta, J.; Niwano, H.; Takezoe, H.; Watanabe, J. *J. Am. Chem. Soc.* **2002**, *124*, 3354.
(35) Dantlgraber, G.; Baumeister, U.; Diele, S.; Kresse, H.; Lühmann, B.; Lang, H.; Tschierske, C. *J. Am. Chem.* Soc. **2002**, *124*, 14852.
(36) Keith, C.; Reddy, A.; Tschierske, C. *Chem. Commun.* **2005**, 871.
(37) Demel, S.; Slugovc, C.; Stelzer, F.; Fodor-Csorba, K.; Galli, G. *Macromol. Rapid Commun.* **2003**, *24*, 636.
(38) Sentman, A. C.; Gin, D. L. *Angew. Chem., Int. Ed.* **2003**, *42*, 1815.
(39) Choi, E. J.; Ahn, J.-C.; Chien, L.-C.; Lee, C.-K.; Zin, W.-C.; Kim, D.-C.; Shin, S.-T. *Macromolecules* **2004**, *37*, 71.
(40) Barberá, J.; Gimeno, N.; Monreal, L.; Piñol, R.; Ros, M. B.; Serrano, J. L. *J. Am. Chem. Soc.* **2004**, *126*, 7190.
(41) Jeong, K. U.; Jin, S.; Ge, J. J.; Knapp, B. S.; Graham, M. J.; Ruan, J.; Guo, M.; Xiong, H.; Harris, F. W.; Cheng, S. Z. D. *Chem. Mater.* **2005**, *17*, 2852.
(42) Knapp, B. S. Ph.D. Dissertation, University of Akron, 2003.
(43) Yoon, Y.; Zhang, A.; Ho, R.-M.; Cheng, S. Z. D.; Percec, V.; Chu, P. *Macromolecules* **1996**, *29*, 294.

(44) Yoon, Y.; Ho, R.-M.; Moon, B.; Kim, D.; McCreight, K. W.; Li, F.; Harris, F. W.; Cheng, S. Z. D.; Percec, V.; Chu, P. *Macromolecules* **1996**, *29*, 3421.
(45) Zheng, R.-Q.; Chen, E.-Q.; Cheng, S. Z. D.; Xie, F.; Yan, D.; He, T.; Percec, V.; Chu, P.; Ungar, G. *Macromolecules* **1999**, *32*, 6981.
(46) Pardey, R.; Shen, D.; Gabori, P. A.; Harris, F. W.; Cheng, S. Z. D.; Adduci, J.; Facinelli, J. V.; Lenz, R. W. *Macromolecules* **1993**, *26*, 3687.
(47) Demus, D. In *Handbook of Liquid Crystals*; Demus, D., Goodby, J., Gray, G. W., Spiess, H.-W., Vill, V., Eds.; Wiley-VCH: Weinheim, 1998; Vol. 1, pp 133−187.
(48) Seddon, J. M. In *Handbook of Liquid Crystals*; Demus, D., Goodby, J., Gray, G. W., Spiess, H.-W., Vill, V., Eds.; Wiley-VCH: Weinheim, 1998; Vol. 1, pp 635−679.
(49) Eashoo, M.; Wu, Z.; Zhang, A.; Shen, D.; Tse, C.; Harris, F. W.; Cheng, S. Z. D.; Gardner, K. H.; Hsiao, B. S. *Macromol. Chem. Phys.* **1994**, *195*, 2207.
(50) Bovey, F. A.; Mirau, P. A. *NMR of Polymers*; Academic Press: San Diego, 1996.
(51) Cheng, J.; Jin, Y.; Wunderlich, B.; Cheng, S. Z. D.; Yandrasits, M. A.; Zhang, A.; Percec, V. *Macromolecules* **1992**, *25*, 5991.
(52) Cheng, J.; Yoon, Y.; Ho, R.-M.; Leland, M.; Guo, M.; Cheng, S. Z. D.; Chu, P.; Percec, V. *Macromolecules* **1997**, *30*, 4688.
(53) McElheny, D.; Grinshtein, J.; Frydman, V.; Frydman, L. *Macromolecules* **2002**, *35*, 3544.
(54) Ishida, H.; Horii, F. *Macromolecules* **2002**, *35*, 5550.
(55) Dierking, I. *Textures of Liquid Crystals*; Wiley-VCH: Weinheim, 2003.
(56) Krigbaum, W. R.; Watanabe, J. *Polymer* **1983**, *24*, 1299.

MA051389J